# A Method to Study Complex Enzyme Kinetics Involving Numerical Analysis of Enzymatic Schemes

Lolkema, Juke S.

*Published in:*
The Journal of Biological Chemistry



*Publication date:*
1993

THE JOURNAL OF BIOLOGICAL CHEMISTRY
© 1993 by The American Society for Biochemistry and Molecular Biology, Inc.

Vol. 268, No. 24, Issue of August 25, pp. 17850-17860, 1993
Printed in U.S.A.

# A Method to Study Complex Enzyme Kinetics Involving Numerical Analysis of Enzymatic Schemes

## THE MANNITOL PERMEASE OF *ESCHERICHIA COLI* AS AN EXAMPLE*

(Received for publication, March 1, 1993)

**Juke S. Lolkema‡**

*From the Department of Microbiology, University of Groningen, Kerklaan 30, 9751 NN Haren, The Netherlands*

**An analysis of complex kinetic mechanisms is proposed that consists of two steps, (i) building of an kinetic scheme from experimental data other than steady-state kinetics and (ii) numerical simulation and analysis of the kinetics of the proposed scheme in relation to the experimental kinetics. Procedures are introduced to deal with large numbers of enzymatic states and rate constants, and numerical tools are defined to support the analysis of the scheme.**

**The approach is explored by taking the mannitol permease of *Escherichia coli* as an example. This enzyme catalyzes both the transport of mannitol across the cytoplasmic membrane and the phosphorylation of mannitol. The challenge is to deduce the transport properties of this dimeric enzyme from the phosphorylation kinetics. It is concluded that (i) the steady-state kinetic behavior is largely consistent with the proposed catalytic cycle of the monomeric subunit, (ii) the kinetics provide no direct support but also do not disprove a coupled translocation of the binding sites on the two monomeric subunits. The approach reveals the need for further experimentation where the implementation of experimental results in the scheme conflict with the experimental kinetics and where specific experimental characteristics do not show up in the simulations of the proposed kinetic scheme.**

The steady-state kinetic performance of an enzyme is a reflection of the mechanism by which the enzyme catalyzes a reaction. The kinetic behavior is a global property of a particular mechanism, and, therefore, this mechanism cannot be directly deduced from the kinetics. To learn about the mechanism from the experimental kinetics, the kinetic performance of hypothetical mechanisms are analyzed theoretically and the results are compared with the experimental behavior. Then, the mechanism for which the theory predicts similar behavior as observed experimentally is assigned to the enzyme under study. For relatively simple kinetic mechanisms there will be a unique relation between kinetic scheme and kinetic performance (*e.g.* "ping-pong," ternary complex, etc).

As kinetic schemes and performances become more complicated two problems arise in the approach outlined above, (i) the analysis of the schemes and, (ii) degeneracy of the solution, *i.e.* more than one kinetic scheme may account for the same kinetic behavior. The theoretical analysis of a scheme results in a rate equation pertinent to a particular mechanism which analytically describes the turnover rate of the enzyme as a function of the concentrations of the ligands that interact with the enzyme, *e.g.* substrates, inhibitors, etc. The analysis involves the solution of sets of linear equations, the number of which equals the number of enzymatic states in the kinetic scheme. This becomes very tedious as the number of equations increases and although the King and Altman method (1) provides significant improvement of such analyses, complex mechanisms involving many states of the enzyme remain difficult to treat analytically. This limits the approach to relatively simple enzyme mechanisms and excludes mechanisms that, for instance, involve cooperativity, multiple pathways, or subunit interactions, that lead to rapidly increasing numbers of states of the enzyme.

The complexity of a kinetic mechanism is immediately evident from the experimental kinetic behavior of an enzyme when the relation between the turnover rate and the ligand concentrations cannot be described by single saturation curves. Especially in those cases, an understanding of the kinetics in terms of the underlying kinetic scheme would contribute significantly to the understanding of the functioning of the enzyme. In this paper, a method is described for the study of complex kinetic mechanisms. The degeneracy problem is dealt with by incorporating results from many different types of experiments other than steady-state kinetics into a hypothetical scheme. The kinetics of the hypothetical scheme are simulated and analyzed numerically. In this way the kinetics of enzyme mechanisms involving almost unlimited numbers of states can be analyzed.

The method is demonstrated by taking the mannitol permease of *Escherichia coli* as an example. This enzyme catalyzes both the transport of mannitol across the cytoplasmic membrane and the phosphorylation of mannitol. The mannitol phosphorylation kinetics of this transport protein can be measured much more accurately than the transport kinetics (2). The challenge will be to deduce the transport properties of this enzyme from the phosphorylation kinetics.

### THE METHOD

Scheme I shows schematically the method that consists mainly of two steps, (i) building of a hypothetical kinetic scheme from data other than steady-state kinetics (left) and (ii) numerical analysis of the kinetic performance of this scheme and, at the same time, comparing the results with the experimental steady-state kinetics (right). The method aims at building a kinetic scheme from many scattered pieces of evidence that is consistent with the steady-state kinetics.

*Building of the Scheme*—The steady-state kinetic performance of an enzyme is not enough to unravel a complex kinetic mechanism. Although the kinetic characteristics are a direct

* This work was supported by the Netherlands Organization for Scientific Research (N. W. O.). The costs of publication of this article were defrayed in part by the payment of page charges. This article must therefore be hereby marked "*advertisement*" in accordance with 18 U.S.C. Section 1734 solely to indicate this fact.

‡ Tel.: 31-50-632155; Fax: 31-50-632154.

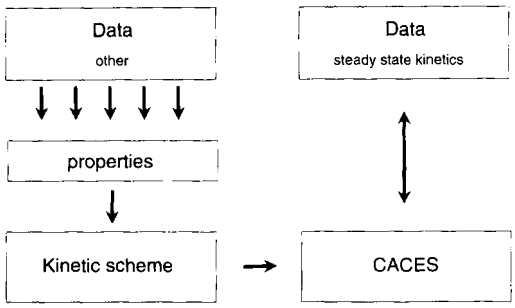


SCHEME I. **General approach.** CACES is the software that simulates and analyzes the kinetic scheme.

property of the underlying mechanism, other mechanisms may result in similar characteristics. More detailed experimental data is necessary that focusses on parts of the overall mechanism. In the approach outlined in Scheme I the kinetic scheme is based largely on this type of data, *i.e.* data other than steady-state kinetics. The "other" data may reflect many different types of experiments, each one assigning specific properties to the enzyme. One by one, these pieces of detailed information are integrated into the kinetic scheme where they may interact to give a particular kinetic behavior. Many of the bits and pieces will rely heavily upon the interpretation of a particular experiment. While some properties assigned to the kinetic scheme may be reasonably well supported by experimental data, other properties may be no more than consistent with the data. The power of the integration process is that, in the end, the kinetic scheme build on all these interpretations must be compatible with the experimental kinetics.

*The Analysis*—CACES (Computer Analysis of Complex Enzymatic Schemes) is a computer program that simulates the kinetic behavior of any hypothetical kinetic scheme under any set of conditions. In addition, tools are built into the software to analyze the kinetic behavior of the scheme (see Experimental Procedures). These tools help to find a set of rate constants pertinent to the hypothetical scheme that makes the kinetic characteristics of the scheme in accord with the experimental data provided there is such a set. Therefore, analyzing the scheme with CACES shows whether or not the properties assigned to the hypothetical scheme are consistent with the steady-state kinetics. A failure to find a consistent set of rate constants may be due to one particular property assigned to the scheme, that, subsequently, may be removed. Alternatively, some unknown property may have to be added to the scheme. A consistent set of rate constants will add new properties to the scheme by virtue of the individual rate constants. At any rate, the analysis will lead to reinterpretation of existing experimental data and proposals for new experiments. At best, a cyclic approach of proposing and testing develops until the kinetic scheme is consistent with both the experimental steady-state kinetics and the other data.

## EXPERIMENTAL PROCEDURES

*Tools for the Analysis of the Kinetic Characteristics*—The numerical solution of the steady-state equations results in the distribution of the enzyme over the $n$ states, $E_{1\ldots n}$. The *turnover rate* of the enzyme ($v$) under a specific set of conditions follows from the distribution of the enzyme over these states. A number of other derivatives of the steady-state distribution may be defined that serve as tools in the analysis of the kinetic characteristics of the scheme.

The *flux fraction* measures the contribution of the flux through one particular transition ($v_{ij}$) to the turnover of the enzyme ($v$). A flux fraction $\phi_{ij}$ may be defined for every transition within the scheme

$$\phi_{ij} = \frac{v_{ij}}{v} = \frac{k^*_{ij}E_i - k^*_{ji}E_j}{v} \qquad \text{(Eq. 1)}$$

Rate constants $k^*_{ij}$ and $k^*_{ji}$ are either first order or pseudo-first order. The flux fraction is the tool to determine the *major pathway* through the scheme by connecting subsequent transitions with high flux fractions. A related parameter is the flux fraction of a subclass of transitions (see below), $\Sigma\phi$, which sums the flux fractions of the transitions in the subclass.

Balance $B_{ij}$ is defined as the ratio of the distribution over states $E_i$ and $E_j$ in the kinetic steady-state and at thermodynamic equilibrium:

$$B_{ij} = \frac{E_j/E_i}{k^*_{ij}/k^*_{ji}} \qquad \text{(Eq. 2)}$$

Balance indicates how far a transition is out of thermodynamic equilibrium. When $B_{ij} = 1$ the transition is at thermodynamic equilibrium.

The *friction coefficient* $f_{i,j}$ of the transition between states $E_i$ and $E_j$ measures the sensitivity of the turnover rate to a change in the free energy of the transition state between $E_i$ and $E_j$ without affecting the free energies of the two states themselves. Friction $F_{i,j}$ in the transition between $E_i$ and $E_j$ may be defined as

$$F_{i,j} = \frac{1}{k_{ij}}\sqrt{K_{ij}} = \frac{1}{k_{ji}}\sqrt{1/K_{ij}} \qquad \text{(Eq. 3)}$$

in which $K_{ij}$ is the ratio of $k_{ij}$ and $k_{ji}$, *i.e.* the equilibrium constant. It then follows for the friction coefficient.

$$f_{i,j} = -\frac{dv/v}{dF_{i,j}/F_{i,j}} \qquad \text{(Eq. 4)}$$

The friction coefficient indicates to which extent the transition between states $E_i$ and $E_j$ determines the flux through the enzyme. In the numerical treatment the friction coefficient is determined by calculating the relative increase in the turnover rate of the enzyme when both $k_{ij}$ and $k_{ji}$ are increased by 1%. If the increase in the turnover rate would be 1%, the transition between states $E_i$ and $E_j$ is completely rate-determining. The friction coefficient is similar to the sensitivity function defined by Ray (3). A more detailed treatment of the friction and the friction coefficient as defined in Equations 3 and 4, respectively, will be published elsewhere.

*The Software*—CACES is a menu-driven, interactive computer program that both simulates and analyzes steady-state kinetics of a predefined enzymatic scheme. The sets of linear equations are solved by Gauss elimination or matrix inversion which are standard computational techniques (4). The enzyme is defined by the number of states and numerical values for the first and second order rate constants. An experimental condition is defined by numerical values for the ligand concentrations. The set of rate constants is checked for thermokinetic balancing (5). Experiments are simulated by repeating the calculations over a range of concentrations of one particular ligand while keeping the other parameters constant and outputting the data in Lineweaver-Burk plots. The flux fraction, balance, and friction coefficient (see above) have been implemented into the software as tools for the analysis of the major pathways, the equilibrium positions, and rate-determining steps in the enzymatic scheme, respectively. Calculated turnover rates may be fitted to known rate equations by a nonlinear fitting procedure using the simplex algorithm (6) followed by analysis of the residuals (7, 8). CACES was written and compiled using the Borland Pascal 7.0 IDE (Borland Inc.) and runs on any AT-type personal computer. The CACES program is available on request.

## THE KINETIC SCHEME

### *The Mannitol Permease of E. coli*

Mannitol transport in *E. coli* is catalyzed by a phosphoenolpyruvate-dependent phosphotransferase system (for reviews, see Refs. 9 and 10). The physiological relevant reaction catalyzed by enzyme $II^{mtl}$, the mannitol-specific transport protein of this system, is

$$\text{Mannitol}_{out} + \text{P-HPr} \xrightarrow{II^{mtl}} \text{mannitol-P}_{in} + \text{HPr} \qquad \text{(Eq. 5)}$$

In addition to transport, the permease catalyzes phosphorylation of mannitol; mannitol appears as mannitol-P inside the cell. The phosphoryl group donating substrate is a small cytoplasmic protein, termed P-HPr. The enzyme $II^{mtl}$ molecule consists of three well defined domains (11–14). Domains IIA and IIB protrude into the cytoplasm while domain IIC is situated in the membrane (15). The phosphoryl group of substrate P-HPr is transferred to mannitol by subsequent phosphorylation of phosphoryl group binding sites on domains IIA and IIB (16). Transmembrane domain IIC contains the mannitol binding site (11, 17).

*Experimental Data Used to Built the Scheme*

1) Both physical and kinetic measurements indicate that enzyme $II^{mtl}$ is a homodimer (18–26). 2) Dissociated monomeric enzyme $II^{mtl}$ catalyzes P-HPr-dependent phosphorylation of mannitol (Equation 5) with a different specific activity (26). 3) Phosphorylation of domain IIA does not effect the mannitol binding properties of domain IIC (27). 4) NMR studies indicate that P-HPr does not bind to phosphorylated domain IIA (28). 5) Translocator domain IIC is activated by phosphorylation of enzyme $II^{mtl}$ (29). 6) Mannitol can bind to unphosphorylated enzyme $II^{mtl}$ in the absence of P-HPr, and P-HPr can phosphorylate enzyme $II^{mtl}$ in the absence of mannitol (17, 19, 24). 7) Membrane bound domain IIC constitutes a mannitol translocator that exposes a single binding site alternately to either side of the membrane (17, 30, 31). 8) Phosphorylation and transport of mannitol are, mechanistically, separate steps (29). 9) Phosphorylated enzyme $II^{mtl}$ catalyzes efflux of mannitol from cells (32). 10) At 4 °C, mannitol binds to membrane vesicles with an inside-out orientation with an affinity constant of 35 nM. Binding to vesicles with a right-side-out orientation indicated a affinity of the periplasmic binding site that was about a factor of 10 lower (30). Binding to purified enzyme $II^{mtl}$ solubilized in detergent revealed two different binding sites per dimer (24). 11) Enzyme $II^{mtl}$ catalyzes phosphorylation of cytoplasmic mannitol (31). 12) The fraction of mannitol bound to the cytoplasmic binding site that is phosphorylated in a single turnover upon the addition of P-HPr is 30–40% ("the mannitol-P burst"). This condition will be referred to as the mannitol-P burst efficiency (29). 13) In the unphosphorylated state, the association/dissociation of mannitol at the cytoplasmic side of the membrane is in the order of minutes, whereas this is considerably faster at the periplasmic side (17, 30). 14) The affinity of enzyme $II^{mtl}$ for the substrate analogue perseitol that cannot be phosphorylated does not change dramatically upon phosphorylation of the enzyme (33). 15) Size exclusion chromatography of the separate domain IIC, and domains IIA and IIB together, demonstrate that the sites of interaction that keep the enzyme $II^{mtl}$ dimer together are exclusively located in membrane bound domain IIC (34).

*Properties of the Kinetic Scheme*

*A Cooperative Dimer*—Enzyme $II^{mtl}$ is a dimer (see above number 1). Dissociated monomeric enzyme $II^{mtl}$ possesses all the machinery necessary to catalyze P-HPr-dependent mannitol phosphorylation. Therefore, the turnover of each monomeric subunit within the dimer constitutes a complete catalytic cycle (number 2). In the associated state the two subunits interact; the two cycles are coupled at one or more steps (number 2).

*The Monomeric Cycle*—Scheme II shows the catalytic cycle of the monomeric subunit. The scheme has been set up to simulate initial rate measurements. The concentration of the two products, mannitol-P and HPr, is zero. Consequently, the

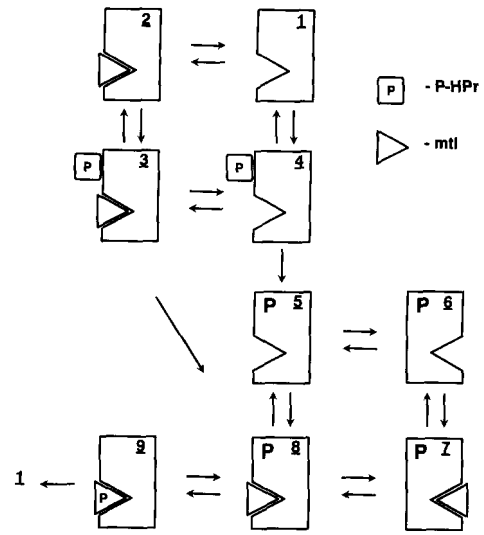


SCHEME II. **Kinetic cycle of the monomeric enzyme $II^{mtl}$.** The *left* and *right* side of each state represent the cytoplasm and periplasm, respectively. The *triangular* notch represents the mannitol binding site. Capitol "P" denotes a phosphoryl group covalently attached to the enzyme.

enzyme-product complexes and the product association steps may be omitted from the scheme. The internal phosphoryl group transfer between the cytoplasmic domains IIA and IIB is ignored. This implies that the different states of phosphorylation of the monomeric subunit do not effect the kinetic behavior of the enzyme (number 3). P-HPr does not bind to phosphorylated enzyme $II^{mtl}$ (number 4).

State *9* is the "productive" state. After dissociation of mannitol-P, the binding site on state *1* does not reorient because the translocator is not activated (number 5). The binding of P-HPr and mannitol is random (number 6). States *5–8* built a facilitated diffusion cycle for mannitol (numbers 7 and 8). It is only active in the phosphorylated state (numbers 5 and 9). Mannitol binds to the cycle at either side of the membrane (numbers 7 and 10). The two orientations of the binding site will be referred to as the periplasmic and cytoplasmic binding site.

The scheme provides two different kinetic pathways for mannitol phosphorylation in a noncompartmentalized system. Mannitol may bind to the periplasmic binding site (steps *6* to *7*) followed by translocation to the inside (state *8*) and phosphoryl group transfer to mannitol (state *9*). Alternatively, the translocation step may be omitted by direct binding of mannitol to the cytoplasmic-facing binding sites (states *1*, *4*, and *5*) followed by phosphorylation (number 11). State *5* is a switch between the two pathways that is controlled by the mannitol concentration. At low mannitol concentrations translocation to state *6* will be favored over binding of mannitol (state *8*).

The rate constant of transition *8* to *5* is about twice as large as the combined rate constant for the combined transitions *8* to *9* to *1* (number 12). Since the latter has to be faster than the turnover number of the enzyme, in the scheme, dissociation of mannitol from phosphorylated enzyme $II^{mtl}$ (step *8* to *5*) is much faster than dissociation from the unphosphorylated enzyme (step *1* to *2*)(number 13). The affinity constants for mannitol of the periplasmic binding site on the phosphorylated and unphosphorylated enzyme are not very different (number 14).

*Functional Coupling of the Translocator Domains*—The two monomeric catalytic cycles are coupled at the level of the translocation cycles (states *5* through *8*, Scheme II) (number

15). Mannitol binding studies are consistent with the view that when the binding site on one subunit faces one side of the membrane the binding site on the other subunit faces the opposite side of the membrane (number 10) (30). In the kinetic scheme the reorientation of one binding site in one direction is in concert with the reorientation of the other site in the opposite direction. This property together with those assigned to the catalytic cycle of the monomer leads to three states of activation of the translocator. The translocator is inactive when both subunits are not phosphorylated and fully active when both are phosphorylated. In between, when only one of the subunits is phosphorylated the translocation activity of the dimer as a whole is diminished since the activated subunit has to drag along the binding site on the nonactivated subunit. The state of activation of the translocator under turnover conditions will depend on the rates of phosphorylation and dephosphorylation of the enzyme and, therefore, on the mannitol and P-HPr concentrations.

*The Two Subunits Are Indistinguishable*—The state in which, for instance, subunit A is phosphorylated and subunit B has bound mannitol is in the same pool of molecules as the state in which subunit A has bound mannitol and subunit B is phosphorylated.

*Defining the Scheme*

The properties assigned to enzyme $II^{mtl}$ result in a total of 36 states (Fig. 1). There are 168 transitions between these states with non-zero rate constants. The first step in controlling this large number of transitions is to classify them according to the type of transition in which they are involved. Two types of main classes are presented in Table I, those that involve binding of a ligand (mannitol binding, P-HPr binding, and mannitol-P binding) and those that do not (enzyme $II^{mtl}$ phosphorylation and translocation). The two rate constants pertinent to each main class are denoted by two successive high case characters (*e.g.* A and B, C and D, etc). Within each of the main classes, transitions are grouped together with identical rate constants. These groups make up the subclasses within a main class. For instance, mannitol binding may be subclassified into binding to the two orientations of the site on the unphosphorylated enzyme (cyt and per, Table I) and on the phosphorylated enzyme (cytP and perP). This results in subclasses A1 to A4 for mannitol dissociation and subclasses B1 to B4 for mannitol association. In case the binding sites on the two subunits interact cooperatively, binding to the enzyme with the other site occupied results in four additional subclasses (cytS, cytPS, perS, and perPS). Each step in the scheme is characterized by a code consisting of a character for the main class and an integer for the subclass (*e.g.* A4). Each code represents a numerical value for the rate constant(s) of the subclass. The main classes (A and B, C and D, etc) are defined by the different states of the enzyme and indicate all possible transitions. The subclassification is a variable within a certain scheme; it assigns values to the rate constants.

The complete kinetic scheme is defined by the transition matrix in Fig. 2. Columns and rows represent the states of the enzymes and the elements indicate the transitions by the code of the subclass.

## RESULTS

*Biphasic Kinetics*—Enzyme $II^{mtl}$ solubilized in detergent shows biphasic kinetics with respect to the mannitol concentration. The biphasicity manifests itself most strongly at saturating P-HPr concentrations (Fig. 1 in Ref. 2). A qualitative explanation for the biphasicity is provided by the different possible pathways through the proposed scheme. At low mannitol concentrations, the high affinity regime, mannitol would bind predominantly to the periplasmic binding site followed by translocation and phosphoryl group transfer to mannitol (route $1 \rightarrow 3 \rightarrow 2 \rightarrow 5$ at high P-HPr, Fig. 1). At high mannitol concentrations, the low affinity regime, the translocation step would be short-circuited by direct binding of mannitol to the cytoplasmic binding site (route $3 \rightarrow 4 \rightarrow 7$). In order for the latter to show up as a second kinetic phase the translocation step should be rate-determining in the high affinity regime.

The set of rate constants listed in Table I termed "free access" contains all experimental data available on the rate constants. Rate constants for which no data was available were chosen such that they do not add new properties to the scheme. Simulation of the mannitol-dependent kinetics with this set of rate constants results in a single kinetic phase. The free access set was arbitrarily constructed to match the high affinity regime of the experimental mannitol-dependent kinetics. However, no set of rate constants that fulfilled all the conditions set by the experiments could be constructed that resulted in the biphasic kinetics observed in the experiments.

The failure to show biphasic kinetics is caused by the condition set by the mannitol-P burst efficiency. The high absolute value for dissociation rate constant $k(2 \rightarrow 1)$ results in little friction in the cytoplasmic binding equilibrium. Already at low mannitol concentrations, mannitol phosphorylation proceeds through binding of mannitol to the cytoplasmic binding site, step $1 \rightarrow 2$, even when the affinity of the cytoplasmic binding site is much lower than the affinity of the periplasmic binding sites (Fig. 3). The flux fraction of the translocation step is low. Analysis of the flux fractions at the lower mannitol concentrations reveals the two major pathways depicted in Scheme IIIA. In both pathways product formation follows from mannitol binding to the cytoplasmic binding sites. No significant flux occurs between the two pathways because the periplasmic binding equilibria are basically at thermodynamic equilibrium (not shown). An increase in the mannitol concentration shifts the contribution to the total flux from the upper to the lower pathway which does not change the kinetic characteristics since both pathways are kinetically equivalent.

Two additional sets of rate constants were constructed from the free access set to make the kinetic performance of the scheme conform the experimental behavior of enzyme $II^{mtl}$ (Table I). In the *restricted access* set the access of the cytoplasmic binding sites for mannitol is restricted which results in a violation of the condition set by the mannitol-P burst efficiency. The affinity of the binding sites in both orientations is high. In the *cooperativity* set of rate constants, negative cooperativity between the two mannitol binding sites on the dimer is introduced. The affinity for mannitol of one site on the dimer is decreased when the other site is occupied. Both the restricted access model and the "cooperativity" model can adequately account for the biphasic kinetics demonstrated by enzyme $II^{mtl}$ when solubilized in detergent (Fig. 4). Analysis of the residuals (7, 8) after fitting the calculated data to the sum of two saturation curves reveals a similar structured deviation as observed with the experimental kinetics indicating similar shapes for the experiment and the simulation (compare Fig. 4 and Fig. 1 in Ref. 2).

The underlying mechanism for the biphasicity is quite different for the two sets of rate constants (Scheme III). The restricted access model behaves according to the tentative qualitative explanation for the biphasicity given above (see Fig. 3). In the high affinity regime the low accessibility of the

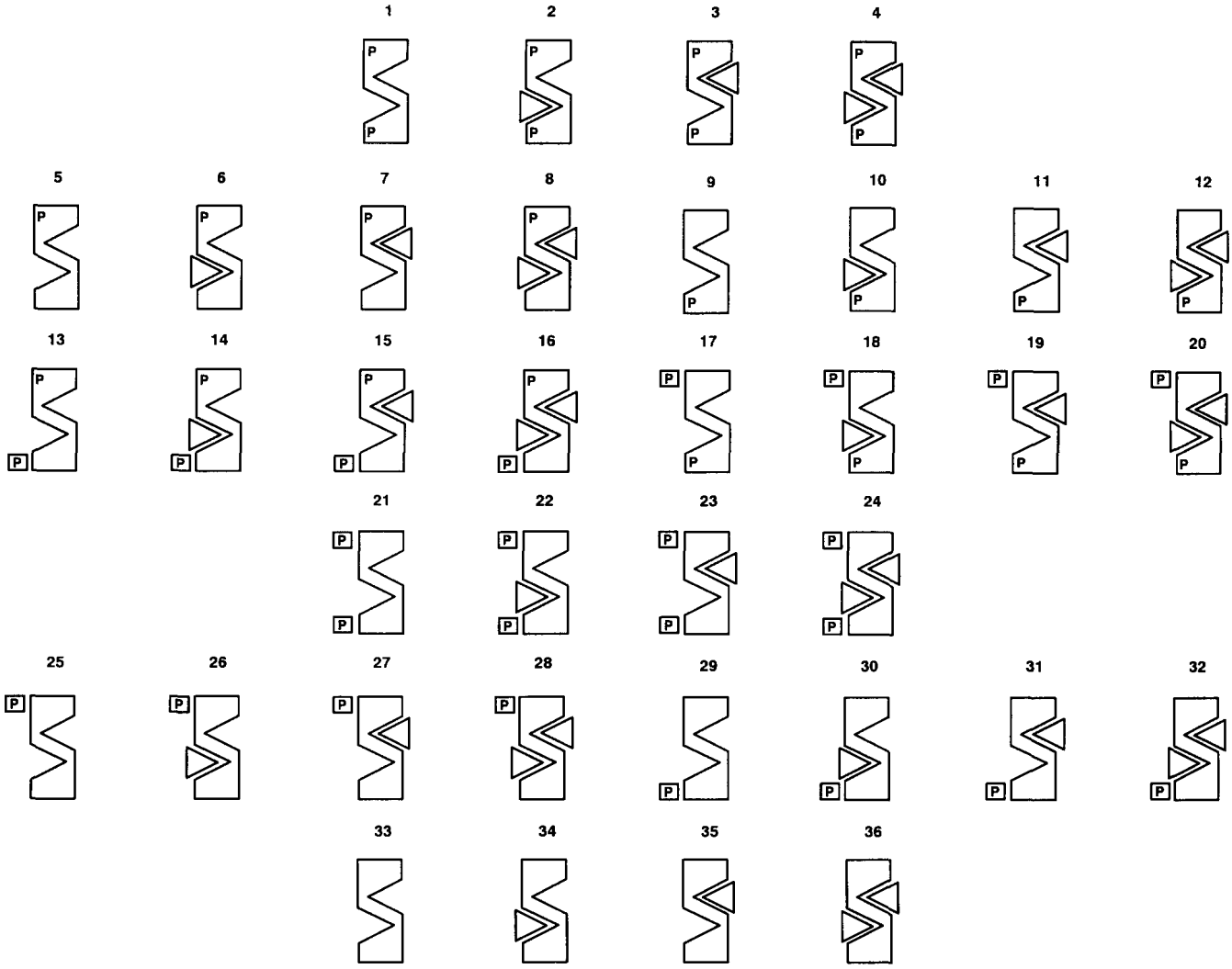


FIG. 1. **The 36 states of dimeric enzyme II$^{mtl}$.** The top and bottom half of each state represent the two subunits. For further explanation, see the legend of Scheme II.

TABLE I

*Three sets of rate constants used in the simulations of the kinetic behavior of the proposed scheme*

Groups and codes are explained in the text. The subclassification of the main classes mannitol binding and translocation relate to each other via thermokinetic balancing. The transitions are defined in Fig. 2. $k_{off}$ and $k_{on}$ refer to the association and dissociation rate constants, respectively, and $k_{fw}$ and $k_{bw}$ to the forward and backward rate constants, respectively. $k_{on}$ is in $\mu M^{-1}$ $s^{-1}$, the other rate constants are $s^{-1}$.

| Binding | Group | Free access | | | | Restricted access | | | | Cooperativity | | | |
|---|---|---|---|---|---|---|---|---|---|---|---|---|---|
| | | $k_{off}$ | | $k_{on}$ | | $k_{off}$ | | $k_{on}$ | | $k_{off}$ | | $k_{on}$ | |
| Mannitol | cytP | A1 | 2000 | B1 | 20 | A1 | 1 | B1 | 0.5 | A1 | 2000 | B1 | 20 |
| | perP | A2 | 100 | B2 | 40 | A2 | 80 | B2 | 40 | A2 | 100 | B2 | 40 |
| | cyt | A3 | 0.1 | B3 | 1 | A3 | 0.1 | B3 | 1 | A3 | 0.1 | B3 | 1 |
| | per | A4 | 40 | B4 | 80 | A4 | 40 | B3 | 80 | A4 | 40 | B4 | 80 |
| | cytPS | A5 | | B5 | | A5 | | B5 | | A5 | 2000 | B5 | 2 |
| | perPS | A6 | | B6 | | A6 | | B6 | | A6 | 100 | B6 | 4 |
| | cytS | A7 | | B7 | | A7 | | B7 | | A7 | 0.1 | B7 | 0.1 |
| | perS | A8 | | B8 | | A8 | | B8 | | A8 | 40 | B8 | 8 |
| P-HPr | | C | 100 | D | 25 | C | 45 | D | 25 | C | 15 | D | 15 |
| Mannitol-P | | E | 1000 | F | | E | 1500 | F | | E | 1000 | F | |
| **Transition** | **Group** | $k_{fw}$ | | $k_{bw}$ | | $k_{fw}$ | | $k_{bw}$ | | $k_{fw}$ | | $k_{bw}$ | |
| EII phosphorylation | | G | 20 | H | | G | 65 | H | | G | 60 | H | |
| Translocation | High | I1 | 400 | J1 | 10 | I1 | 25 | J1 | 25 | I1 | 400 | J1 | 10 |
| | LowSS | I2 | 1 | J2 | 5 | I2 | 0.2 | J2 | 1 | I2 | 1 | J2 | 5 |
| | LowSP | I3 | 2 | J3 | 2 | I3 | 1 | J3 | 1 | I3 | 2 | J3 | 2 |
| | LowS | I4 | 8 | J4 | 1 | I4 | 0.2 | J4 | 1 | I4 | 8 | J4 | 1 |
| | Low | I5 | 4 | J5 | 0.1 | I4 | 1 | J5 | 1 | I5 | 40 | J5 | 1 |

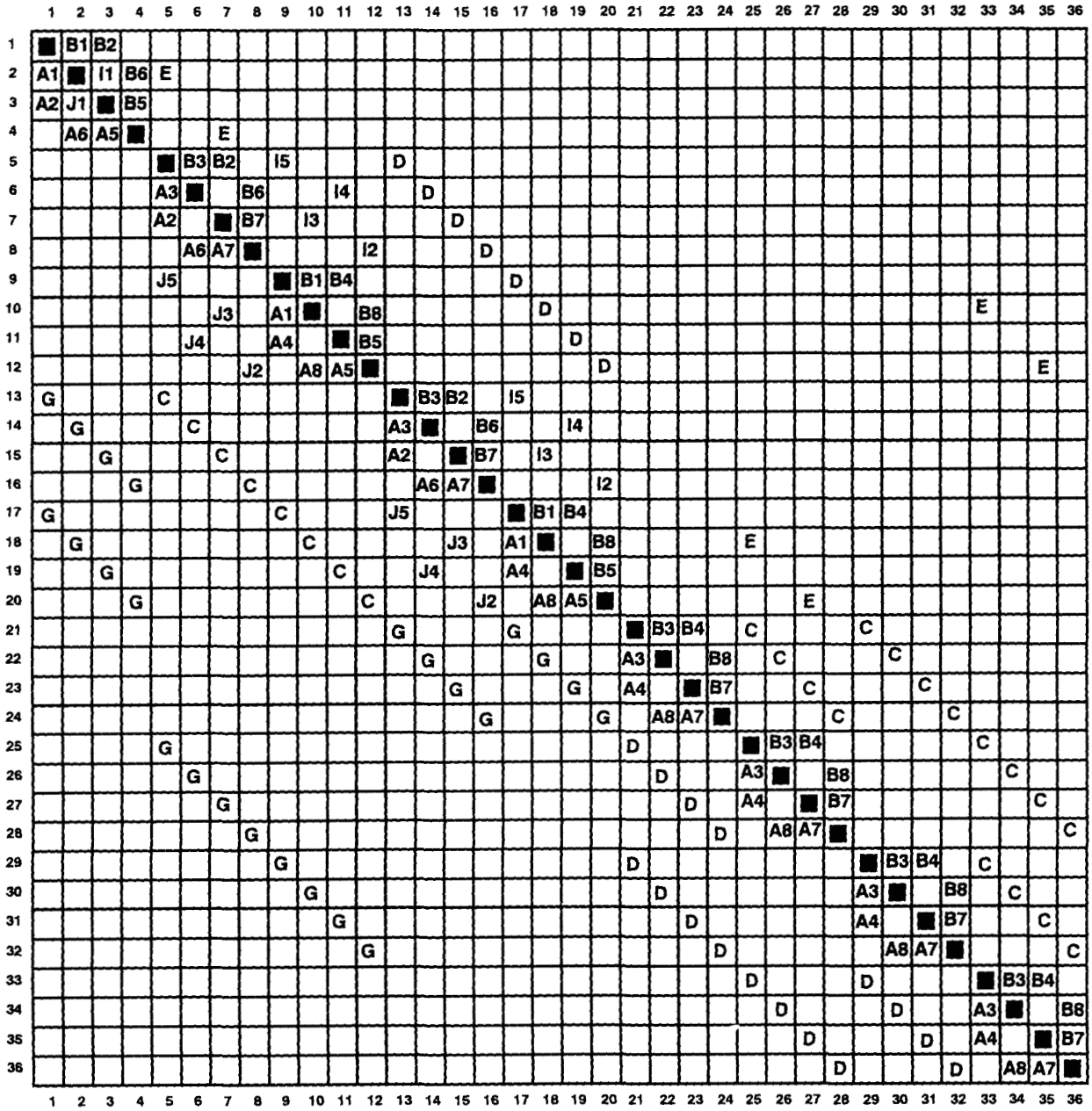

FIG. 2. **Definition of the kinetic scheme; the transition matrix.** The states in Fig. 1 are listed from left to right and from top to bottom. Each element represents a rate constant according to the code given in Table I. Groups A5 through A8 and B5 through B8 are identical to groups A1 through A4 and B1 through B4, respectively, when no cooperativity is assumed between the two mannitol binding sites.

cytoplasmic binding site is overcome by binding to the periplasmic binding site followed by translocation to form productive state *2* (Scheme IIIB). The high friction coefficient of the translocation step indicates that the kinetic regime is mainly determined by this step. In the low affinity regime, the high concentrations of mannitol compensate for the low accessibility of the cytoplasmic binding site. The flux is through the cytoplasmic binding sites, thereby, bypassing the friction in the translocation step (Fig. 3). In the cooperativity model, product formation follows both in the high and low affinity regime predominantly from binding to the cytoplasmic binding sites (Fig. 3). After binding of mannitol to the periplasmic site (Scheme IIIC), binding to state *3* to form productive state *4* is unfavorable because of the negative cooperativity between the two binding sites. Translocation to state *2* is unfavorable because the translocation equilibrium ($3 \leftrightarrow 2$) is far to state *3*, a consequence of thermokinetic balancing (Table I). Instead, mannitol dissociates from the periplasmic binding site followed by binding to the cytoplasm-oriented binding site which is no longer hindered by the negative cooperativity. High concentrations of mannitol compensate for the low affinity of the cytoplasmic site when the periplasmic site is occupied and the flux will be through the cytoplasmic binding sites as well (Fig. 3).

*Mannitol Phosphorylation by Inside-out Membrane Vesicles*—In a compartmentalized system like an inside-out vesicle, mannitol inside the vesicles and mannitol outside the vesicles are different substrates. The steady-state concentration of internal mannitol will be reached very rapidly because of the very small internal volume of these vesicles. The internal concentration of mannitol is set by enzyme $II^{mtl}$ at a value that makes the rates of association and dissociation to

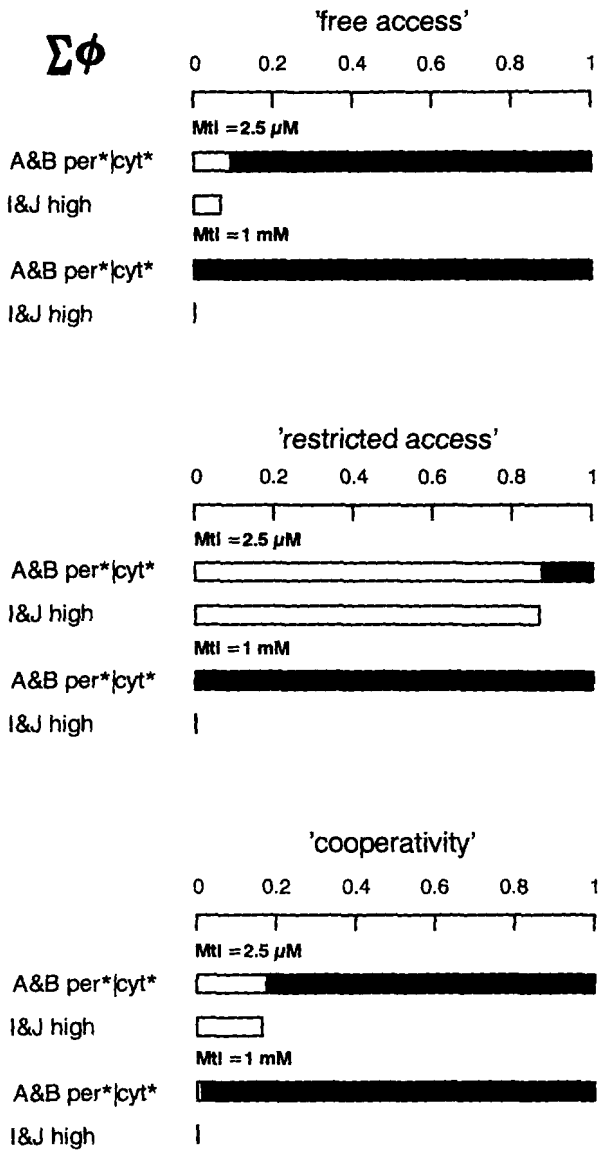


FIG. 3. **Flux fractions of the mannitol binding equilibria (*A&B*) and the high activity translocation (*I&J high*).** In the case of the mannitol binding equilibria, the *open left part* of the bar and the *solid right part* of the bar indicate the flux fractions through the periplasmic and cytoplasmic binding steps, respectively. $\Sigma\phi(per^*) = \Sigma\phi(per + perP + perS + perPS)$ and $\Sigma\phi(cyt^*) = \Sigma\phi(cyt + cytP + cytS + cytPS)$. Note that $\Sigma\phi(per^*) + \Sigma\phi(cyt^*) = 1$. The P-HPr concentration was 24 μM.

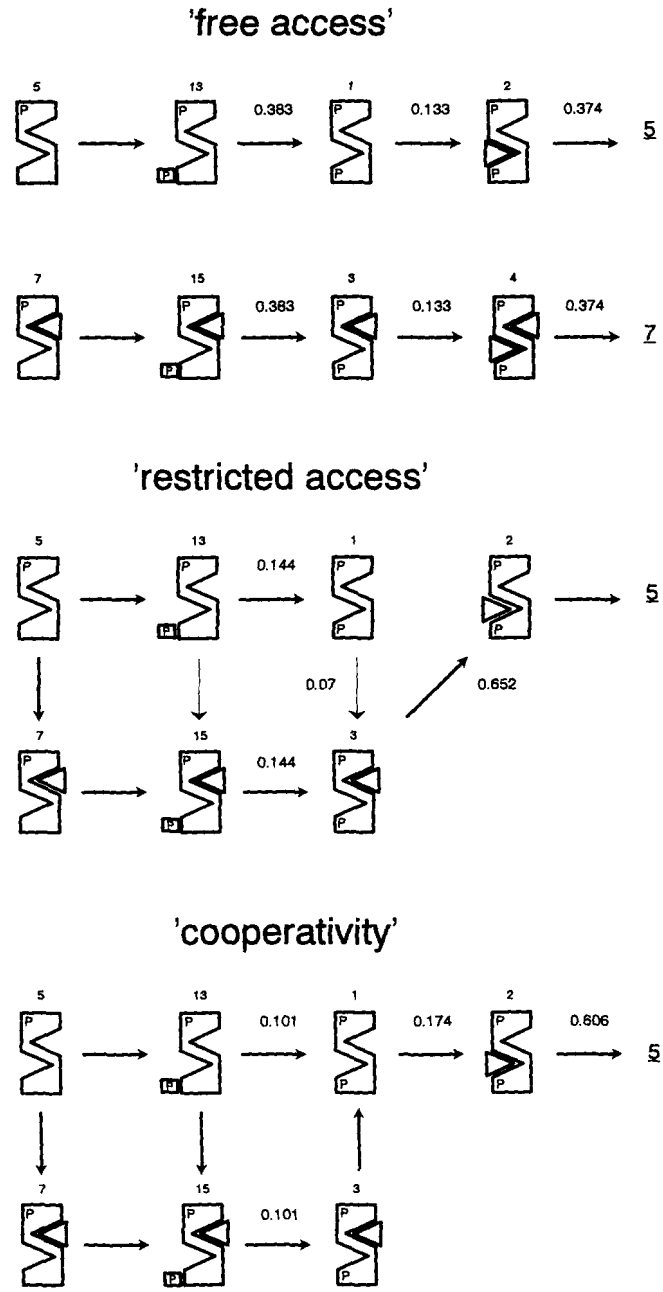


SCHEME III. **Major pathways with the free access (*A*), the restricted access (*B*), and the cooperativity (*C*) set of rate constants.** The mannitol and P-HPr concentrations were 2.5 and 24 μM, respectively. A value of 0.1 for the flux fraction of a transition was used as a threshold to designate the transition part of the major pathway. The three highest friction coefficients are indicated. Note that the friction coefficient is identical for all transitions within a subclass.

and from the internal, periplasmic binding sites equal in the steady-state. Using this criteria, the value of the internal mannitol concentration in the steady-state may be found by an iterative procedure. At a fixed external concentration, the internal concentration is varied until the flux fractions of the periplasmic binding equilibria equal zero. The rate of mannitol phosphorylation is calculated from the distribution under this condition. This rather time consuming procedure can be circumvented by setting the periplasmic association/dissociation rate constants to zero.

It was argued in the accompanying paper (2) that the mannitol-dependent phosphorylation kinetics of enzyme $II^{mtl}$ embedded in the membrane of vesicles with an inside-out orientation is characterized by a single low affinity phase. The affinity for mannitol would be in the same order of magnitude as the affinity in the low affinity regime of the kinetics of the solubilized enzyme. The maximal rate would be identical to the maximal rate observed with the solubilized enzyme.

Simulation of the mannitol phosphorylation kinetics catalyzed by inside-out vesicles discriminates strongly between the restricted access model and the cooperativity model (Fig. 5). In the inside-out vesicles the flux is forced through the cytoplasmic binding sites. With the solubilized enzyme in the cooperativity model, the major pathway was through the cytoplasmic binding sites over the whole range of mannitol concentrations and, therefore, the kinetic behavior is roughly the same with the inside-out vesicles (Fig. 5*B*). In contrast, with the solubilized enzyme in the restricted access model,

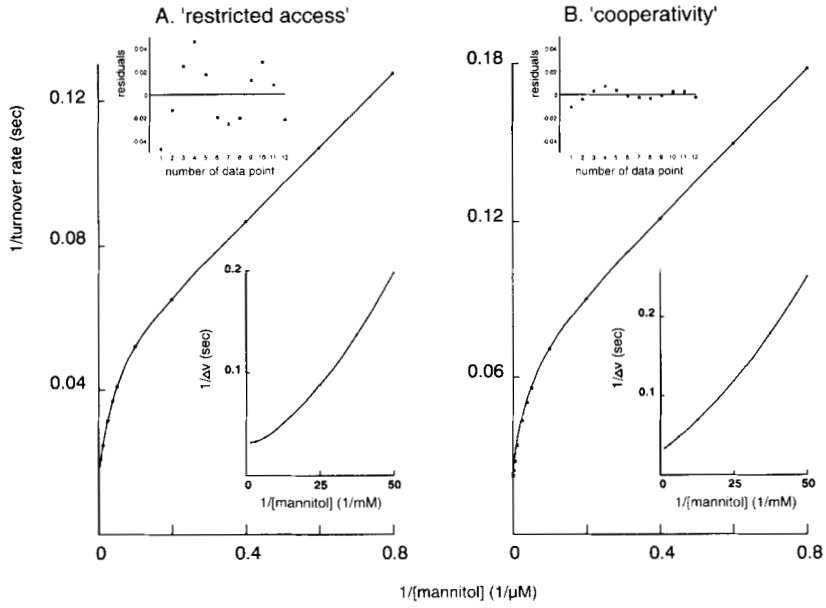


FIG. 4. **Simulations of the biphasic kinetics.** The *top inset* shows the residual analysis after a nonlinear fit of the data to the sum of two saturation curves. The *bottom inset* shows the kinetic characteristics of the low affinity regime that was computed from the difference between the turnover rate and the extrapolated turnover rate from the high affinity regime. The P-HPr concentration was 24 μM.

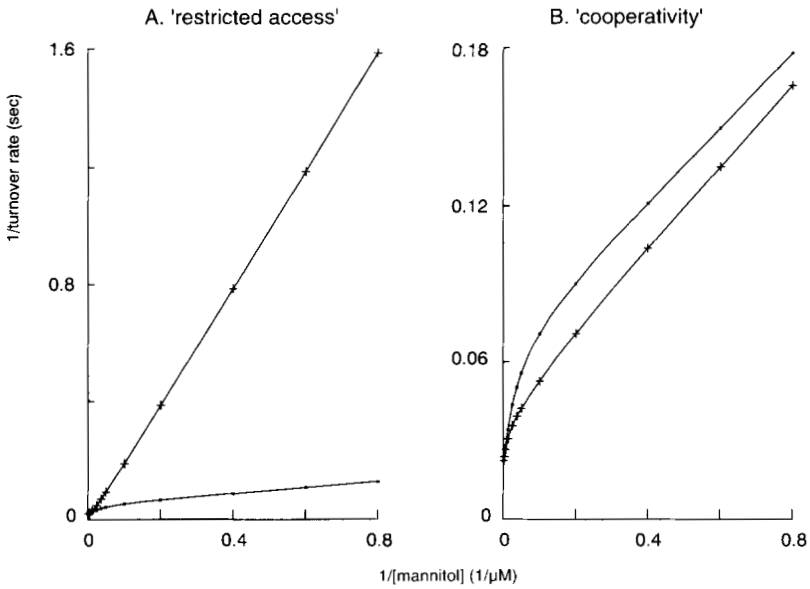


FIG. 5. **Simulations of the kinetics of mannitol phosphorylation catalyzed by the enzyme solubilized in detergent (·) or embedded in the membrane of inside-out vesicles (+).** The P-HPr concentration was 24 μM.

the major pathway was via the periplasmic binding sites in the high affinity regime, resulting in a much lower rate at the lower mannitol concentrations with the inside-out vesicles. A single phase with a low affinity results (Fig. 5*A*, +). At the higher mannitol concentrations, the pathway is identical to that observed with the solubilized enzyme, resulting in the same maximal rate. In conclusion, the restricted access model gives a good fit to the experimental behavior of enzyme $II^{mtl}$ embedded in the membrane of inside-out vesicles, whereas the cooperativity model fails to predict the experimental behavior.

*Conformational Coupling between the Binding Sites*—The combination of the activation of the translocator by phosphorylation of the enzyme and the coupled movement of the two binding sites resulted in the high and low activity translocation modes depending on the degree of phosphorylation of the enzyme. Qualitatively, it may be argued that this property may explain the drop in the phosphorylation rate in the high affinity regime upon lowering the P-HPr concentration (Figs. 2 and 4 in Ref. 2). In the high affinity regime of the restricted access model the rate is at high P-HPr concentrations determined by the translocation between states *2* and *3* that is of the high activity type. Decreasing the P-HPr concentration and, thereby, the steady-state degree of phosphorylation of the enzyme would shift the rate-determining step from the high to the low activity translocation modes.

Simulating the effects of a decreasing P-HPr concentration within the restricted access model does not show the expected behavior. Lineweaver-Burk plots of the rate of mannitol phosphorylation as a function of the mannitol and P-HPr concentrations show sets of parallel lines in the high affinity regime, as is the case for a classical ping-pong mechanism. Analysis of the friction coefficients in the scheme shows that when the P-HPr concentration is decreased, the friction in the scheme shifts from the high activity translocation step to the steps that lead to the phosphorylation of the enzyme (Fig. 6). The degree of phosphorylation of the enzyme is only decreased when the enzyme phosphorylation steps become rate-determining. The expected increase of the flux fraction through the low activity translocation steps is only limited ($\Sigma\phi$(lowSS

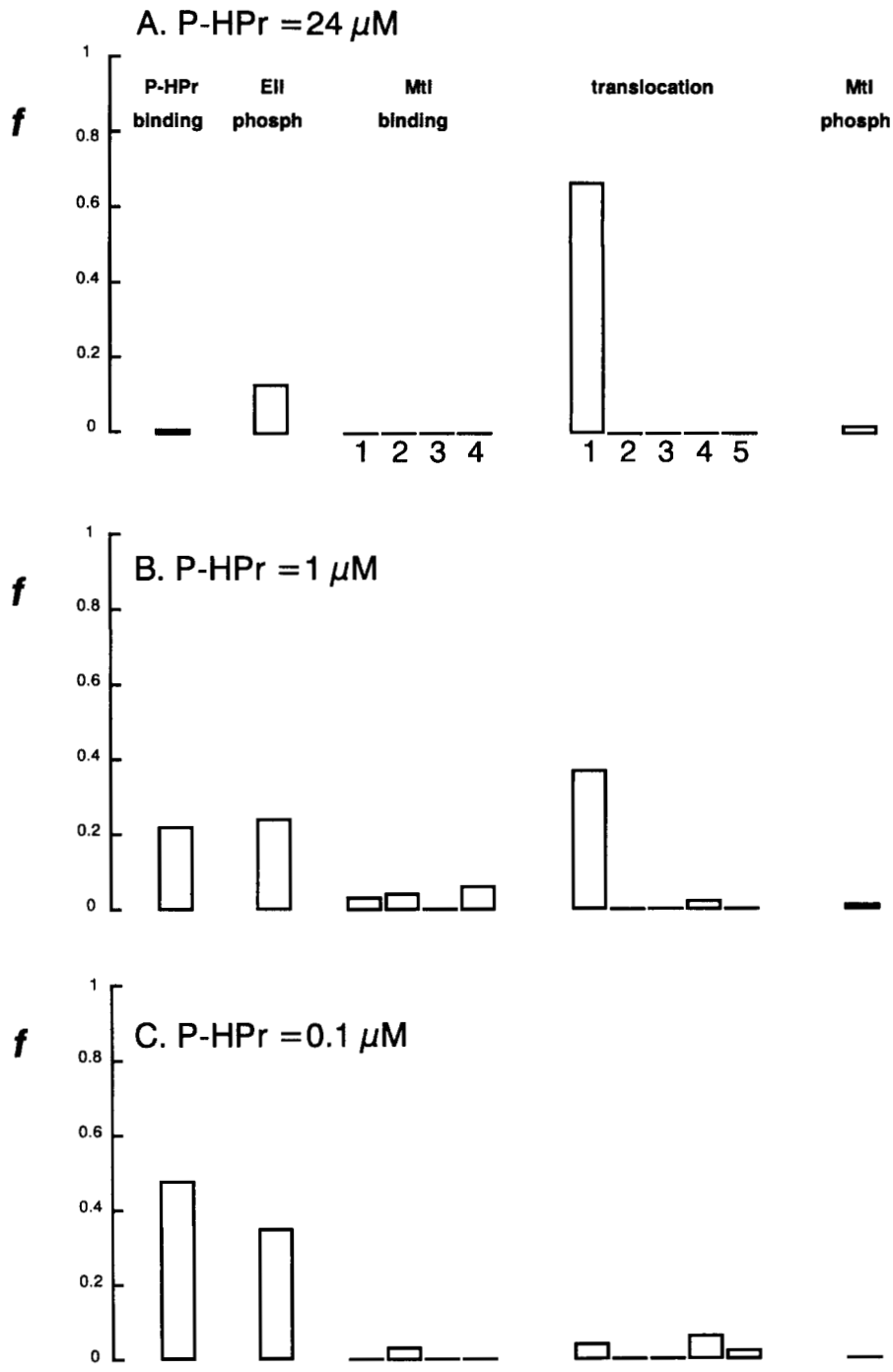


FIG. 6. **The friction coefficient of the subclasses in the high affinity regime at 24 μM (*A*), 1 μM (*B*), and 0.1 μM P-HPr (*C*) in the restricted access model.** The subclassifications of mannitol binding and translocation is according to Table I.

+ lowSP + lowS + low) = 0.0017 and 0.22 at P-HPr = 24 and 0.1 μM, respectively) but, more importantly, the friction coefficients of these steps are small (Fig. 6). The P-HPr dependence of the phosphorylation rate in the high affinity regime provides no direct support for the property of the coupled translocation of the binding sites.

*Inhibition of Translocation*—Dilution of solubilized enzyme $II^{mtl}$ from above to below the cmc[1] of the detergent results in a drastic change of the kinetic characteristics. It was argued that this could be due to an inhibition of translocation of the binding sites (2).

Simulation of the mannitol phosphorylation activity in the restricted access model with the translocation rate constants set to zero shows a striking resemblance with the experimental behavior (compare Fig. 7 with Fig. 5 in Ref. 2). The key property of the scheme responsible for this behavior is the slow association step of mannitol to the cytoplasmic binding site which makes the friction coefficient in this step high over a wide range of mannitol concentrations. The plateau in each line indicates the region in which the steps leading to the phosphorylation of the enzyme become rate-determining. The experiments indicated a maximal rate of mannitol phosphorylation that was a factor of two higher for enzyme $II^{mtl}$ below the cmc as compared to above the cmc. The simulations do not show this increase.

## DISCUSSION

*Sets of Rate Constants*—Much of the experimental data that was used to build the hypothetical scheme for enzyme

[1] The abbreviation used is: cmc, critical micellular concentration.

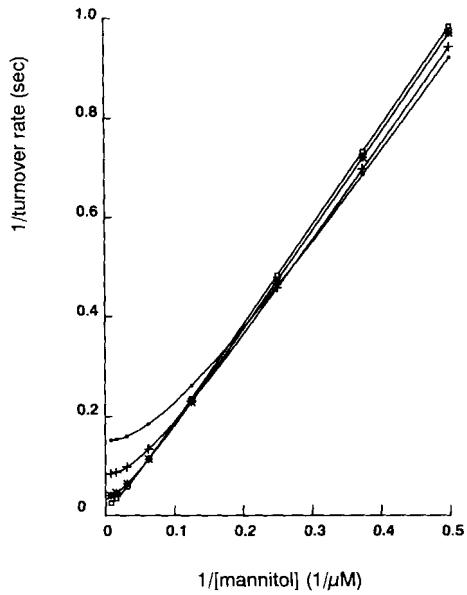


FIG. 7. **Simulations of the kinetics of mannitol phosphorylation by the enzyme diluted under the cmc of the detergent with the restricted access set of rate constants.** The translocation rate constants were set to zero. The simulations were performed with concentrations of P-HPr of 12 (□), 3 (*), 1 (+), and 0.5 (■) μM.

$II^{mtl}$ identifies states of the scheme, *i.e.* association state, enzyme-substrate complexes, phosphorylated intermediates, etc. Possible transitions between these states are based upon both experiment and rationale. Much more than the scheme itself, the dynamics of the scheme is determined by the set of rate constants for the transitions between the states in the scheme. The free access set strictly followed the available experimental data and did not add properties to the scheme for which their was no experimental evidence. However, this set failed to explain the biphasic kinetics with respect to the mannitol concentration, a pronounced feature of the enzyme $II^{mtl}$ kinetics. Two additional sets of rate constants were constructed from the free access set. The restricted access set violated the condition set by the mannitol-P burst efficiency. The cooperativity set added a new property to the scheme: cooperativity between the binding sites. The biphasic kinetics could be simulated with both sets. However, in a next step, the "cooperativity model" clearly was incompetent to simulate the kinetics of the enzyme embedded in the membrane of inside-out vesicles.

*The Restricted Access Model*—This predicts correctly, (i) the biphasic mannitol-dependent kinetics, (ii) the affinity of the solubilized enzyme for P-HPr (not shown), (iii) the mannitol phosphorylation kinetics of inside-out vesicles, and (iv) the kinetics of the solubilized enzyme below the cmc. The model fails to predict, (i) the P-HPr-dependent kinetics in the high affinity regime, (ii) the increase in the maximal rate of the enzyme below the cmc as compared to above the cmc.

The essential properties of the scheme with the restricted access set of rate constants that are responsible for the kinetic behavior are, (i) the existence of a cytoplasmic and periplasmic pathway leading to the phosphorylation of mannitol, (ii) the activation of translocation by phosphorylation of the monomeric subunit, (iii) the random binding of P-HPr and mannitol to the unphosphorylated subunit, (iv) the slow mannitol binding equilibrium at the cytoplasmic binding site.

The restricted access set of rate constants violates the condition set by the mannitol-P burst efficiency. About two-thirds of the mannitol molecules bound to the cytoplasmic binding sites were not trapped as mannitol-P upon the addition of P-HPr but seemed to dissociate into the cytoplasm. It was concluded that phosphorylation of the enzyme enhanced the dissociation rate constant of bound mannitol to the same order of magnitude as the overall rate constant for the transfer of the phosphoryl group to mannitol (27). The simulations show that this conclusion is at variance with the biphasic kinetics exhibited by enzyme $II^{mtl}$. It seems to be essential that the experimentally determined slow association/dissociation of mannitol at the cytoplasmic binding site in the unphosphorylated state (17, 30) is not dramatically effected by phosphorylation of the enzyme.

*Monomer or Dimer*—Up to now, no reference has been made to the discussion on the coupled movement of the binding sites or even to the dimeric structure. The restricted access model does not provide direct support for these properties. In fact, implementation of the essential features of the restricted access model listed above in the monomeric cycle described in Scheme II results in a kinetic scheme with the same kinetic behavior. A pronounced structural property like the conformational coupling between two subunits does not show up in the functioning of the enzyme at the kinetic level. It should be noted that the steady-state kinetics does not disprove the dimeric structure. A dimer with coupled binding sites is consistent with the kinetics to the extent described above. The dimer was introduced in the scheme based upon other types of experiments. The failure of the proposed scheme to explain the 2-fold increase in maximal rate after dilution of the solubilized enzyme under the cmc of the detergent might be a manifestation of the dimeric structure of the enzyme. Possibly, the dilution results in two identical subunits, both with the binding site fixed at the cytoplasmic side of the enzyme, resulting in a 2-fold increase of catalytic units.

*The Approach*—The approach described in this paper results in a catalytic cycle for the monomeric subunit of enzyme $II^{mtl}$ that is supported by a lot of experimental data. The coupled movement of the binding sites on the dimer are consistent with the kinetics, but the kinetics provides no proof for the correctness of this property. It may serve as a working hypothesis for future experimentation. The interpretation of the mannitol-P burst efficiency needs to be reevaluated and requires further experimentation. The inability of the scheme to explain the P-HPr-dependent kinetics may reflect properties of the enzyme for which no experimental evidence is available to date. Possibly, the simplifying contraction of the two phosphorylation sites on one subunit may not be justified. Recently, domains IIB and IIC were subcloned from the gene coding for enzyme $II^{mtl}$ and expressed as one protein that appears to be fully active in mannitol phosphorylation when phosphorylated domain IIA is used as substrate.[2] In this assay system the internal phosphoryl group transfer on enzyme $II^{mtl}$ is omitted and the kinetic characteristics may show whether the P-HPr dependence relates to different degrees of phosphorylation of the monomeric subunits of enzyme $II^{mtl}$.

*Acknowledgments*—I thank Drs. George Robillard and Bert Poolman for critical reading of the manuscript and many helpful suggestions.

REFERENCES

1. King, E. L., and Altman, C. (1956) *J. Phys. Chem.* **60,** 1375
2. Lolkema, J. S., ten Hoeve-Duurkens, R. H., and Robillard, G. T. (1993) *J. Biol. Chem.* **268,** 17844–17849
3. Ray, W. J. (1983) *Biochemistry* **22,** 4625–4637
4. *Turbo Pascal Toolbox Numerical Methods* (1987) pp. 105–129, Matrix

[2] H. de Boer and G. T. Robillard, unpublished results.

Routines, Borland International, Scotch Valley, CA
5. Walz, D., and Caplan, S. R. (1988) *Cell Biophys.* **12,** 13–28
6. Nelder, J. A., and Mead, R. (1965) *Comput. J.* **7,** 308
7. Bartfai, T., and Mannervik, B. (1972) *FEBS Lett.* **26,** 252–256
8. Mannervik, B., Gorna-Hall, B., and Bartfai, T. (1973) *Eur. J. Biochem.* **37,** 270–281
9. Postma, P. W., and Lengeler, J. W. (1985) *Microbiol. Rev.* **49,** 232–269
10. Lolkema, J. S., and Robillard, G. T. (1992) *New Compr. Biochem.* **21,** 135–168
11. Grisafi, R. L., Scholle, A., Sugayama, J., Briggs, L., Jacobson, G. R., and Lengeler, J. W. (1989) *J. Bacteriol.* **171,** 2719–2727
12. White, D. W., and Jacobson, G. R. (1990) *J. Bacteriol.* **172,** 1509–1515
13. van Weeghel, R. P., Meyer, G. H., Pas, H. H., Keck, W. H., and Robillard, G. T. (1991) *Biochemistry* **30,** 9478–9485
14. van Weeghel, R. P., Meyer, G. H., Keck, W. H., and Robillard, G. T. (1991) *Biochemistry* **30,** 1774–1779
15. Stephan, M. M., and Jacobson, G. J. (1986) *Biochemistry* **25,** 8230–8234
16. Pas, H. H., and Robillard, G. T. (1988) *Biochemistry* **27,** 5835–5839
17. Lolkema, J. S., Swaving Dijkstra, D., ten Hoeve-Duurkens, R. H., and Robillard, G. T. (1990) *Biochemistry* **29,** 10659–10663
18. Saier, M. H. (1980) *J. Supramolec. Struct.* **14,** 281–294
19. Roossien, F. F., and Robillard, G. T. (1984) *Biochemistry* **23,** 5682–5685
20. Stephan, M. M., and Jacobson, G. R. (1986) *Biochemistry* **25,** 4046–4051
21. Roossien, F. F., van Es-Spiekman, W., and Robillard, G. T. (1986) *FEBS Lett.* **196,** 284–290
22. Pas, H. H., Ellory, J. C., and Robillard, G. T. (1987) *Biochemistry* **26,** 6689–6696
23. Khandekar, S. S., and Jacobson, G. R. (1989) *J. Cell. Biochem.* **39,** 207–216
24. Pas, H. H., ten Hoeve-Duurkens, R. H., and Robillard, G. T. (1988) *Biochemistry* **27,** 5520–5525
25. Roossien, F. F., Blaauw, M., and Robillard, G. T. (1984) *Biochemistry* **23,** 4934–4939
26. Lolkema, J. S., and Robillard, G. T. (1990) *Biochemistry* **29,** 10120–10125
27. Lolkema, J. S., Swaving Dijkstra, D., ten Hoeve-Duurkens, R. H., and Robillard, G. T. (1991) *Biochemistry* **30,** 6721–6726
28. van Nuland, N. A. J., Kronn, G. J. A., Dijkstra, K., Wolters, G. K., Scheek, R. M., and Robillard, G. T. (1993) *FEBS Lett.* **315,** 11–15
29. Lolkema, J. S., ten Hoeve-Duurkens, R. H., Swaving Dijkstra, D., and Robillard, G. T. (1991) *Biochemistry* **30,** 6716–6721
30. Lolkema, J. S., Swaving Dijkstra, D., and Robillard, G. T. (1992) *Biochemistry* **31,** 5514–5521
31. Elferink, M. G. L., Driessen, A. J. M., and Robillard, G. T. (1990) *J. Bacteriol.* **172,** 7119–7125
32. Solomon, E., Miyai, K., and Lin, E. C. C. (1973) *J. Bacteriol.* **172,** 723–728
33. Lolkema, J. S., Wartna, E., and Robillard, G. T. (1993) *Biochemistry* **32,** 5848–5854
34. Lolkema, J. S., Kuiper, H., ten Hoeve-Duurkens, R. H., and Robillard, G. T. (1993) *Biochemistry* **32,** 1396–1400